Journal of African Earth Sciences 57 (2010) 31–40

Contents lists available at ScienceDirect

Journal of African Earth Sciences

journal homepage: www.elsevier.com/locate/jafrearsci

Sr–Nd isotopes and geochemistry of granite-gneiss complexes from the Meatiq and Hafafit domes, Eastern Desert, Egypt: No evidence for pre-Neoproterozoic crust

Jean-Paul Liégeois [a,*], Robert J. Stern [b]

[a] Isotope Geology, Royal Museum for Central Africa, Leuvensesteenweg 13, B-3080 Tervuren, Belgium
[b] Geosciences Department, University of Texas at Dallas, Richardson, TX 75080-3021, USA

ARTICLE INFO

Article history:
Received 25 September 2008
Received in revised form 2 July 2009
Accepted 5 July 2009
Available online 16 July 2009

Keywords:
Neoproterozoic juvenile crust
Nd model ages
Rb–Sr isochrons
Arabian–Nubian Shield
Greater gondwana
Eastern Desert gneiss complexes

ABSTRACT

Neoproterozoic gneisses at Meatiq and Hafafit in the Eastern Desert of Egypt give Rb–Sr and U–Pb zircon ages of 600–750 Ma. These gneisses are interpreted by different workers to represent deeper levels of juvenile Neoproterozoic crust or Archaean/Palaeoproterozoic crust that was remobilized during Neoproterozoic time. Geochemical and Sr–Nd isotope compositions for these gneisses reported here are remarkably homogeneous: Initial $^{87}Sr/^{86}Sr$ (0.70252 ± 0.00056) and ε_{Nd} (+6.4 ± 1.0). These values are best explained as reflecting derivation from depleted asthenospheric mantle sources during Neoproterozoic time, consistent with mean Nd model ages of 0.70 ± 0.06 Ga. The increasing recognition of old, xenocrystic zircons in juvenile ANS igneous rocks can be explained in several different ways. The participation of ancient crust is allowed as one of the explanations, but it is the isotopic composition of radiogenic elements such as Sr and Nd for whole-rock specimens that are the most reliable indicators of whether or not a given crustal tract is juvenile or reworked older crust. These isotopic data indicate that the protolith for the Meatiq and Hafafit gneisses were juvenile Neoproterozoic igneous rocks and sediments derived from them. There is no support in the isotopic data for any significant contribution of pre-Neoproterozoic crust in these two sections of Eastern Desert crustal infrastructure.

1. Introduction

Crust of NE Africa comprises the eastern part of the Archaean/Palaeoproterozoic Saharan metacraton (SmC) partly reworked during Neoproterozoic time (Abdelsalam et al., 2002) and the mostly Neoproterozoic Arabian–Nubian Shield (ANS), which is characterized by the abundance of ophiolites and fossil juvenile island arcs (Abdelsalam and Stern, 1996; Johnson and Woldehaimanot, 2003). The position and nature of the boundary between the two domains is controversial but lies near or within the Eastern Desert of Egypt (Fig. 1). Traditional views for the Eastern Desert infer that scattered exposures of high-grade metamorphic rocks (infrastructure) reveal a deep substrate of the SmC ("fundamental basement" of Hume, 1934) and that larger regions exposing low-grade metamorphic rocks and oceanic-related rocks (superstructure) reveal allochthonous ANS slices. In more recent versions of this interpretation, Eastern Desert ophiolites and related rocks (Fig. 1) are considered to have been thrust west over >1.8 Ga continent (gneiss complexes in Fig. 1), the uprise and exposure of the latter being a late Neoproterozoic post-collisional feature (e.g., El-Gaby et al., 1984). However, geochronological and isotopic data increasingly challenge this interpretation. First, Eastern Desert gneisses yield radiometric ages of 800–600 Ma by both the zircon evaporation technique (Kröner et al., 1994; Bregar et al., 2002) and zircon TIMS method (Andresen et al., 2009). These zircon ages show no evidence of older inherited zircons. Second, the inference that high-grade infrastructure is tectonically covered by a low-grade superstructure has been recently challenged in the Egyptian Eastern Desert (El Sibai complex; Fowler et al., 2007).

All parties to this controversy recognize that Archaean and Palaeoproterozoic rocks of the SmC can be found to the west at Uweynat in SW Egypt and SE Libya (Harris et al., 1984 and references therein; Fig. 1A), in scattered basement exposures west of the Nile (Sultan et al., 1994) and even as close to the Eastern Desert as Wadi Halfa on the Nile just south of the border with Sudan (Stern et al., 1994; Fig. 1A). Farther south in the Sudan, high-grade felsic rocks and granitoids in the Bayuda Desert (Fig. 1A) have recently been shown to be 920–900 Ma old but with a clear Palaeoproterozoic inheritance (SHRIMP U–Pb zircon and Nd model ages; Küster et al., 2008). These rocks are in tectonic contact with c. 700–800 Ma amphibolite-facies oceanic island arc rocks (Küster and Liégeois, 2001; Küster et al., 2008). In Sudan, the tectonic boundary between the SmC and the ANS is exposed, marked by the Keraf suture (Abdelsalam and Stern, 1996; Fig. 1A).

The controversy about the age and origin of ANS infrastructure continues, for good reasons and bad. There are clearly extensive

* Corresponding author. Tel./fax: +32 2 650 2252.
E-mail addresses: jean-paul.liegeois@africamuseum.be (J.-P. Liégeois), rjstern@utdallas.edu (R.J. Stern).

1464-343X/$ - see front matter © 2009 Elsevier Ltd. All rights reserved.
doi:10.1016/j.jafrearsci.2009.07.006

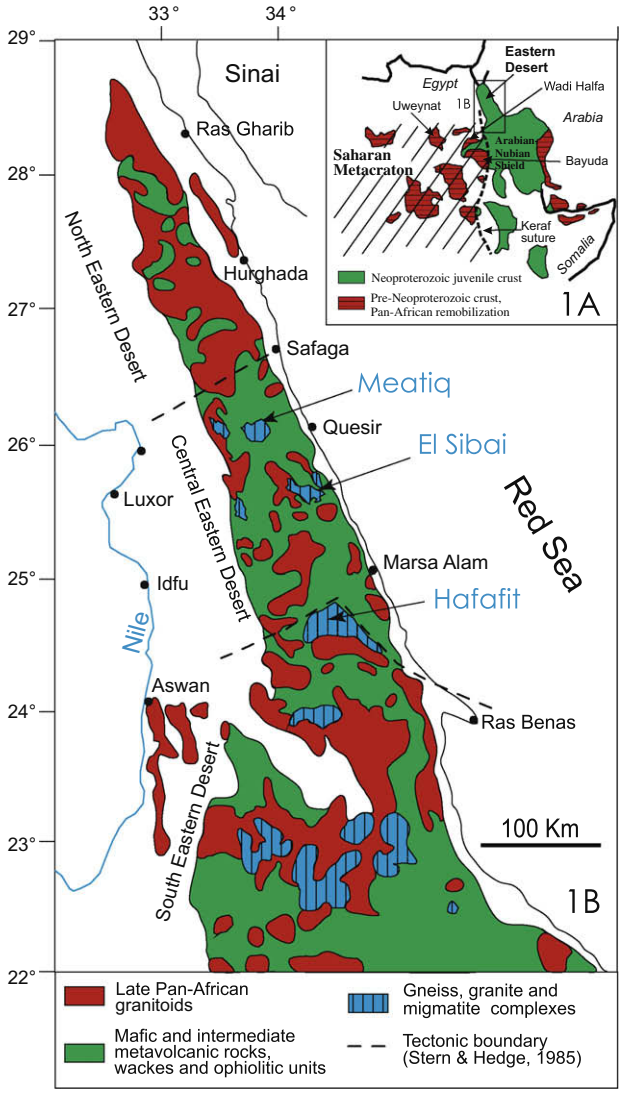

Fig. 1. (A) Geological sketch map of NE Africa showing the juvenile Arabian–Nubian Shield and the Saharan metacraton, mostly a pre-Neoproterozoic crust variably remobilized during the Neoproterozoic. Location of the studied area is marked by a rectangle and the regions cited in the text are marked. (B). Map of the three main Precambrian basement subdivisions of the Eastern Desert in Egypt with the location of the two studied gneissic complexes, Meatiq and Hafafit.

tracts of remobilized crust of Palaeoproterozoic and Archaean age in Yemen (Whitehouse et al., 2001a) and in the Khida terrane of the Arabian Shield (Whitehouse et al., 2001b). These metamorphic rocks show clear isotopic as well as geochronological evidence of their pre-Neoproterozoic age. Direct evidence that pre-Neoproterozoic crust was nearby is revealed by ~750 diamictite, which contains clasts up to a meter in size, many of which have ~1.8 and ~2.5 Ga ages; these probably formed as a result of Sturtian glaciation (Ali et al., 2009a). In addition, pre-Neoproterozoic zircons are increasingly recognized in juvenile Neoproterozoic ANS igneous rocks. U–Pb dating reveals abundant xenocrystic zircons with ages of especially ~1.9 and ~2.5 Ga (Hargrove et al., 2006a; Kennedy et al., 2004, 2005; Kennedy et al., 2007, submitted for publication; Ali et al., 2009b). Such zircons are found mostly in juvenile Neoproterozoic rocks, i.e., samples with Nd isotopic characteristics indicating derivation by melting of depleted (asthenospheric) mantle and geochemical characteristics suggesting formation in an intra-oceanic arc (Hargrove et al., 2006b).

Xenocrystic zircons are proportionately most abundant in mafic lavas. This is especially the case in the Eastern Desert where relatively abundant Palaeoproterozoic and Archaean xenocrystic zircons have been found in metamorphosed Neoproterozoic basalts, gabbros, andesites and diabases (Ali et al., 2009b). These observations indicate that the distribution and significance of xenocrystic zircons in the otherwise juvenile ANS crust merits further investigation, but it must be stressed that the presence of abundant pre-Neoproterozoic zircons only indicates the presence of older zircons, not the presence of extensive tracts of older crust. These issues are discussed in greater detail below.

Less compelling inferences that pre-Neoproterozoic crust exist beneath the Eastern Desert continued in a recent and unusual interpretation of Sr–Nd isotopic data for Eastern Desert gneisses (Khudeir et al., 2008). We will show here that Sr–Nd isotopes unequivocally demonstrate that Eastern Desert basement gneisses represent juvenile late Neoproterozoic crust, a conclusion that cannot be challenged by the presence of inherited pre-Neoproterozoic zircons present in some associated supracrustal rocks.

2. Geological information

Gneisses exposed in the Eastern Desert reflect an important metamorphic peak, preserved in exhumed deep crust. There are several gneissic complexes in the Eastern Desert (Fig. 1), the two most important of which, the Hafafit and Meatiq complexes, are focused on here. Hafafit comprises the largest gneiss terrane in the Eastern Desert, whereas Meatiq gneisses have long been suspected of representing pre-Neoproterozoic crust or sediments (El-Gaby et al., 1984). Both gneisses are especially appropriate to be studied isotopically to test the hypothesis that the Eastern Desert of Egypt is juvenile Neoproterozoic crust. Geological details on these gneissic complexes can be found in Sturchio et al. (1983), Sultan et al. (1987), Stern and Hedge (1985), Loizenbauer et al. (2001), Bregar et al. (2002), Neumayer et al. (2004), Fowler et al. (2007), Khudeir et al. (2008), Moussa et al. (2008) and Andresen et al. (2009).

It is important to briefly summarize what is known about the metamorphic history of the Meatiq and Hafafit gneiss complexes; metamorphism of the former is much better documented than the latter. Neumayer et al. (2004) found that the Meatiq basement was affected by three metamorphic events (M1, M2, and M3), only the last of which affected the overlying ophiolitic nappes. M1 metamorphism ($T \geqslant 750$ °C) is only preserved in amphibolite xenoliths in the Um Baanib orthogneiss, which comprises the structurally lowest part of the gneiss dome. The age of the Um Baanib orthogneiss is controversial. Andresen et al. (2009) obtained a concordant TIMS U–Pb zircon age of 631 ± 2 Ma, which agrees reasonably well with a five-point Rb–Sr whole-rock isochron of 626 ± 2 Ma (initial $^{87}Sr/^{86}Sr = 0.7030 \pm 1$) reported by Sturchio et al. (1984) for the orthogneiss. Loizenbauer et al. (2001) reported a zircon evaporation $^{207}Pb/^{206}Pb$ age of 779 ± 4 Ma (average of four grains) for this orthogneiss, and single zircon ages of 834 ± 21, 800 ± 4, and 1149 ± 25 Ma for an ortho-amphibolite xenolith. Andresen et al. (2009, pers. comm., 2008) obtained younger ages from mafic enclaves in the Um Baanib orthogneiss. They note that the "enclave" is probably a late intrusion. Andresen et al. (2009, pers. comm., 2008) were not able to reproduce any of the ages obtained by Loizenbauer et al. (2001). M2 was also characterized by upper amphibolite-facies conditions, with local development of kyanite in metasediments. Peak P–T conditions ranged from 610–690 °C at 6–8 kbar; relic kyanite indicates pressures above 8 kbar occurred before thermal maximum was reached. These P–T conditions indicate that Meatiq basement at this stage (between 630 and 580 Ma ago) lays 20–25 km deep, well within the middle crust or uppermost lower crust. Retrograde M2 mineral assemblages formed during the rise of the Meatiq gneisses from this depth. M3 temperatures were not greater than 460–550 °C, associated

Table 1
Major and trace elements were analysed by inductively coupled plasma–mass spectrometry (ICP–MS) in the Geochemical Laboratory of the Royal Museum for Central Africa in Tervuren, Belgium. See Liégeois et al. (2003) for more information. Abu Z. = Abu Ziran; grd = granodiorite; migm = migmatite; foliated bi gr = foliated biotite granite. NYTS-X = mean of Zr–Ce–Sm–Y–Yb and NYTS-Y = mean of Rb–Th–U–Ta, both following the sliding normalization of Liégeois et al. (1998).

Complex	Meatiq										Hafafit				Complex	Hafafit												
Unit	Arieki		Abu Z	Um Baanib					Meatiq		Siqat				Unit	Siqat		Hafafit			Hafafit			Hafafit				Hafafit
Lithology	Late granite		Grd	Gneissic granite			Enclave		Paragneiss		Gneissic grante				Lithology	Gneissic granite		Foliated leucogranite			Amphibolite			Foliated bi granite				Migm
Sample	EB16	EB17	EB1	EB3	EB6	EB7	EB4	EB8	EB9	EB10	EB18	EB19	EB20	EB22	Sample	EB23	EB24	EB27	EB33	EB34	EB26	EB35	EB36	EB30	EB31	EB32	EB37	EB29
SiO_2	73.91	73.99	61.45	76.06	77.34	77.05	50.71	46.43	78.72	73.56	73.74	72.4	72.84	72.56	Sr	72.39	73.59	75.8	77.13	75.52	51.78	47.48	52.51	77.74	77.48	76.02	76.34	69.87
TiO_2	0.18	0.23	0.87	0.26	0.20	0.09	1.37	3.31	0.20	0.33	0.24	0.29	0.25	0.23	Y	0.19	0.27	0.08	0.18	0.19	1.19	0.29	1.49	0.31	0.30	0.31	0.28	0.26
Al_2O_3	13.81	13.97	19.05	12.54	11.72	11.55	11.58	15.27	10.77	11.64	13.65	13.81	13.96	14.28	Al_2O_3	14.37	13.60	13.93	12.05	13.28	18.79	19.47	17.17	11.00	11.36	12.14	11.14	16.42
Fe_2O_3	0.90	0.88	1.78	1.60	1.60	2.24	3.49	3.38	2.72	3.25	0.86	0.89	0.69	0.91	Fe_2O_3	0.74	0.65	0.30	0.90	0.91	0.88	1.35	1.70	2.45	2.49	1.82	2.18	1.08
FeO	0.57	0.78	2.82	0.42	0.34	0.23	7.35	10.31	1.61	0.28	1.47	1.84	1.64	1.65	FeO	1.78	1.91	0.42	0.34	0.25	5.87	4.42	6.23	0.86	0.78	1.08	0.99	1.49
MnO	0.03	0.03	0.04	0.01	0.01	0.01	0.10	0.16	0.03	0.04	0.02	0.03	0.02	0.04	MnO	0.04	0.02	0.01	0.01	0.01	0.09	0.07	0.08	0.03	0.02	0.03	0.03	0.03
MgO	0.25	0.28	0.19	0.04	0.08	0.04	10.52	5.70	0.29	0.12	0.19	0.22	0.19	0.16	MgO	0.11	0.21	0.12	0.11	0.10	5.56	8.73	5.95	0.01	0.06	0.07	0.01	0.89
CaO	1.05	1.11	4.31	0.04	0.37	0.16	10.10	9.18	0.04	1.02	1.20	1.27	1.16	1.30	CaO	1.01	1.08	1.40	0.40	0.52	11.31	13.29	9.50	0.10	0.16	0.28	0.36	4.34
Na_2O	4.03	3.89	5.88	4.63	4.30	4.32	2.84	3.85	0.11	4.23	4.54	4.65	4.54	4.81	Na_2O	4.69	4.50	4.05	4.39	4.38	3.35	2.10	3.86	4.55	4.42	4.80	4.44	4.32
K_2O	4.30	4.30	1.87	4.29	4.15	4.27	0.26	0.26	3.06	4.12	3.82	3.83	4.20	3.89	K_2O	4.41	3.96	4.34	4.95	5.05	0.16	0.13	0.28	3.33	3.38	3.79	3.21	0.59
P_2O_5	0.06	0.06	0.21	0.05	0.04	0.05	0.16	0.57	0.04	0.08	0.08	0.06	0.09	0.08	P_2O_5	0.08	0.05	0.04	0.09	0.07	0.07	0.01	0.16	0.05	0.08	0.05	0.06	0.05
P.F.	0.64	0.73	1.10	0.63	0.59	0.43	2.16	1.53	1.79	1.23	0.99	1.04	0.86	0.75	P.F.	0.82	0.88	0.37	0.39	0.44	1.67	2.16	1.97	0.37	0.40	0.54	0.70	0.69
Total	99.73	100.25	99.57	100.57	100.74	100.44	100.64	99.95	99.38	99.90	100.80	100.33	100.44	100.66	Total	100.63	100.72	100.86	100.94	100.72	100.72	99.50	100.90	100.80	100.93	100.93	99.74	100.03
Rb	157	139	39.3	70.4	61.7	140	9.64	10.56	181	76.5	182	165	154	198	Rb	212	164	61.0	31.5	36.9	9.27	7.56	12.4	37.9	37.8	44.4	44.2	33.5
Sr	86.6	116	1078	30.1	18.9	6.8	312	458	13.4	31.8	75.4	75.4	74.7	75.4	Sr	76.9	69.5	137	26.1	50.0	352	169	466	31.9	77.1	33.2	21.2	251
Y	61.5	55.3	17.1	107	101	189	35.4	45.3	374	143	76.6	88.9	79.3	74.1	Y	96.7	88.7	11.8	8.34	4.22	8.31	8.73	28.5	148	106	144	149	10.5
Zr	161	190	274	639	365	805	126	305	2416	1019	272	339	272	268	Zr	349	312	80.9	182	153	9.69	26.8	104	968	1009	997	1092	204
V	9.00	10.90	67.0	6.80	4.10	1.70	271	237	1.69	2.40	7.00	7.70	6.30	4.30	V	1.11	5.70	1.60	0.19	1.14	155	89.0	156	0.21	0.15	0.76	0.47	31.0
Ba	425	533	887	642	539	19.4	129	118	65.6	747	329	317	331	302	Ba	382	317	696	1657	2009	59.7	64.3	235	893	1294	672	1028	222
La	26.4	36.0	18.1	76.5	67.0	54.7	9.6	25.2	171	103	37.0	43.2	38.6	36.6	La	58.9	40.6	26.7	27.7	32.7	1.72	0.40	10.5	51.7	86.9	106.5	79.6	25.5
Ce	65.2	79.3	44.3	180.6	159.9	132.7	29.8	68.6	420	240	86.2	102	85.1	88.2	Ce	135	96.4	55.0	61.8	74.5	4.71	1.20	29.0	128.0	224	264	216	60.5
Pr	7.64	9.55	5.96	21.8	21.5	17.4	4.86	9.63	59.5	30.3	10.1	12.3	10.8	9.9	Pr	14.8	12.1	5.57	7.83	8.44	0.75	0.28	4.14	16.8	31.7	32.0	29.4	7.03
Nd	29.5	36.8	26.1	90.9	85.5	67.7	25.3	45.6	266	127	40.9	50.0	42.1	39.9	Nd	58.3	44.8	21.3	27.5	31.5	4.40	2.20	20.1	76.5	134	144	122	27.6
Sm	6.28	7.24	4.82	18.11	18.90	17.65	6.04	9.25	66.6	24.0	8.99	10.36	9.21	7.57	Sm	11.82	9.93	3.78	4.50	4.64	1.28	0.82	4.84	17.2	24.6	26.2	23.7	4.24
Eu	0.71	0.81	1.66	2.33	2.27	1.11	1.71	3.29	7.68	4.88	0.87	1.02	0.94	1.21	Eu	1.64	1.00	0.60	1.52	1.69	1.18	0.49	1.90	3.58	5.07	3.77	4.86	0.86
Gd	5.84	5.83	3.44	16.5	15.9	17.1	5.12	7.70	56.6	19.9	8.03	9.19	7.95	7.00	Gd	11.28	9.34	2.88	2.93	2.92	1.17	0.78	4.26	13.6	19.3	23.6	22.4	3.04
Dy	7.87	7.47	2.87	16.8	17.4	27.4	5.91	7.42	62.7	22.0	10.1	11.4	10.1	8.62	Dy	15.2	12.3	2.01	1.58	1.00	1.56	1.43	4.34	21.5	19.5	21.6	22.6	2.01
Ho	1.81	1.60	0.61	3.50	3.38	6.03	1.21	1.60	12.4	4.60	2.25	2.55	2.16	2.13	Ho	3.55	2.61	0.40	0.26	0.19	0.31	0.29	0.97	4.82	4.13	4.77	4.99	0.40
Er	5.54	4.86	1.62	9.23	9.27	17.8	3.24	4.13	32.9	13.1	6.13	7.12	6.51	6.46	Er	10.43	7.93	1.06	0.83	0.52	0.84	0.88	2.37	14.3	11.3	11.9	14.6	1.13
Yb	6.22	5.15	1.45	7.89	7.46	16.4	2.78	3.60	32.5	11.9	5.71	7.14	6.61	7.96	Yb	9.12	7.18	1.00	0.75	0.42	0.72	0.89	2.32	14.9	9.9	10.6	12.7	1.00
Lu	1.00	0.77	0.22	1.15	1.06	2.44	0.38	0.54	4.74	1.8	0.81	1.11	1.00	1.23	Lu	1.22	1.13	0.16	0.11	0.10	0.11	0.12	0.32	2.08	1.65	1.71	2.07	0.17
Hf	4.93	6.09	5.71	15.35	9.44	26.1	3.26	6.14	70.1	22.4	9.10	10.43	9.00	7.73	Hf	9.39	9.81	2.92	4.97	3.90	0.31	0.69	2.53	22.7	20.9	22.2	22.3	5.18
Ta	3.31	2.40	0.59	3.56	2.34	8.01	0.27	1.86	15.4	5.3	6.42	6.32	4.97	9.73	Ta	7.28	5.18	0.10	0.15	0.10	0.10	0.10	0.30	2.42	0.65	0.22	1.73	0.22
Nb	33.9	24.5	9.79	60.5	43.8	138	7.3	28.8	230	83.5	52.0	56.0	47.9	60.0	Nb	149.9	59.0	3.42	2.36	2.10	1.44	0.33	3.70	42.4	21.3	16.8	32.1	3.30
W	0.43	0.62	0.11	0.25	0.72	0.32	0.41	0.56	1.71	0.72	3.02	1.42	0.77	0.66	W	3.11	5.63	0.22	0.10	0.10	0.46	0.43	0.77	0.10	0.30	0.14	0.05	0.12
Pb	16.5	14.1	8.35	5.24	8.44	9.19	1.30	8.57	35.9	7.49	23.8	15.9	16.0	15.8	Pb	17.8	15.1	21.00	13.8	14.9	5.10	1.61	4.84	16.4	13.1	5.4	13.7	6.64
Th	18.1	16.9	2.09	8.80	7.60	14.1	0.30	1.74	33.1	11.2	14.7	18.1	16.8	26.3	Th	59.8	18.7	18.04	7.62	6.58	0.10	0.10	0.70	7.71	4.45	2.48	5.39	7.60
U	9.67	5.75	1.28	2.21	2.43	6.99	0.10	0.45	11.7	4.01	4.10	6.72	7.14	9.07	U	21.3	7.55	2.81	1.16	0.45	0.30	0.10	0.59	3.29	2.19	1.74	2.56	0.98
NYTS-X	1.45	1.47	0.57	3.83	3.61	5.81	–	–	–	4.76	1.83	2.07	1.84	1.76	NYTS-X	2.29	2.09	0.62	0.96	0.72	–	–	–	5.80	5.67	5.31	6.24	0.60
NYTS-Y	1.67	1.25	0.48	1.05	0.77	2.35	–	–	–	1.56	2.02	2.21	1.92	3.23	NYTS-Y	4.03	2.00	0.49	0.22	0.18	–	–	–	0.80	0.34	0.23	0.60	0.31

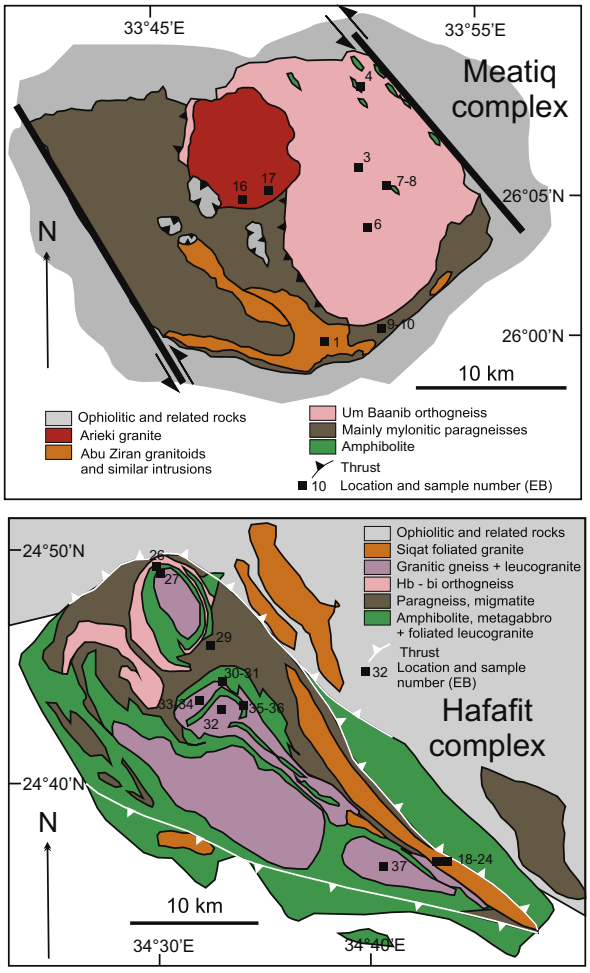

Fig. 2. Simplified geological map for the Meatiq complex (A) and Hafafit complex (B), with the location of the studied samples. Meatiq map from Loizenbauer et al. (2001) and Khudeir et al. (2008); Hafafit map from Abd El-Naby and Frisch (2006) and Fowler and El Kalioubi (2002).

with the updoming of Meatiq basement ~580 Ma ago. This exhumation was linked to sinistral strike-slip movements along Najd shear zones and is dated with $^{40}Ar/^{39}Ar$ techniques on hornblende and mica at 579–595 Ma (Fritz et al., 1996, 2002). This age is consistent with an upper limit of tectonic activity in Meatiq constrained by the undeformed post-kinematic Arieki granitoid, which yielded a TIMS U–Pb age of 590 ± 3 Ma (Andresen et al., 2009) and by concordant titanite ages in several Meatiq lithologies (c. 590 Ma; Andresen et al., 2009).

We have a much more incomplete understanding of the metamorphic evolution of the Hafafit gneiss complex (see Fowler and El Kalioubi, 2002 for a recent summary), but it seems roughly similar to that of Meatiq. In particular, $^{40}Ar/^{39}Ar$ ages for hornblende separates from two Hafafit gneiss samples yielded ages of 584–586 Ma (Fritz et al., 2002), indicating that at least uplift and cooling occurred about the same time as Meatiq.

The lithologies of the studied rocks can be found in Table 1 and their location in Fig. 2. When available for the concerned unit, zircon ages are given in Table 2. For the Meatiq complex, we use TIMS single zircon ages from Andresen et al. (2009) rather than the evaporation zircon ages from Loizenbauer et al. (2001), used only when no TIMS age is available. For the Hafafit complex, we used the evaporation ages of Kröner et al. (1994), the only available zircon ages. We recognize that zircon evaporation ages are valid only if the analyzed crystal is concordant and that condition cannot be verified. The discrepancies existing between some zircon evaporation ages of Loizenbauer et al. (2001) and the zircon TIMS ages of Andresen et al. (2009) can either be attributed to discordant zircons or to a problem of common lead correction, the evaporation technique being hardly able to properly measure the small ^{204}Pb needed for common Pb corrections.

The available zircon U–Pb ages for these gneissic rocks (Kröner et al., 1994; Loizenbauer et al., 2001; Andresen et al., 2009) mostly give ages for protoliths between 700 and 590 Ma, although some paragneiss protoliths are c. 780 Ma (Table 2). Inherited pre-Neoproterozoic zircons are rare in these Eastern Desert gneisses: one strongly discordant zircon fraction from a psammitic gneiss in the Sikait area (Eastern Hafafit complex) has given an upper intercept at 1751 ± 84 Ma (recalculated with Isoplot software, Ludwig, 2003), the other 12 fractions clustering around an unreasonably young age of 420 Ma (Abdel-Monem and Hurley, 1979).

3. Some geochemical characteristics

Data and analytical techniques can be found in Table 1.

Most of the studied samples are granitoids or gneissic granitoids, only a few are metasediments. They are rich in alkalies, belonging to either medium or high-*K* calc-alkaline or alkaline suites (Fig. 3A). Both chemistries are indeed represented as shown by the peralkaline index (Fig. 3B): the Um Baanib orthogneiss, the Hafafit late leucogranite, the Hafafit granitic gneiss and one Meatiq paragneiss are close to the alkaline/peralkaline boundary while the other samples are more akin to the high-*K* calc-alkaline series (peralkaline index <0.87; Liégeois et al., 1998). This is confirmed by using the sliding normalization proposed by Liégeois et al. (1998) that minimizes the effect of the magmatic differentiation: it can be seen that the studied rocks belong to both potassic and alkaline series but that each group is geochemically homogeneous (Fig. 3C). These diagrams use potentially mobile elements (alkali elements, U) but in the case of Meatiq and Hafafit rocks, the coherent behaviour of these elements indicates that there was little elemental redistribution. Plotting sample data on a classical discrimination diagram based on the behaviour of two immobile elements (Y and Nb, Pearce et al., 1984) confirms the above conclusion: the potassic and alkaline samples defined in Fig. 3C fall within the within plate granite field (where post-collisional granites also plot; Liégeois et al., 1998) while samples close to the origin in Fig. 3C plot within the volcanic arc granite field. This is somewhat surprising for the Hafafit leucogranite, which plots close to the alkaline-peralkaline boundary (Fig. 3C). However, evolved peralkaline granites can crystallize minerals that can, through filter pressing, generate granites depleted in some elements such as Nb–Ta (Hadj Kaddour et al., 1998).

The studied rocks present a variety of rare earth element (REE) patterns, but like the major elements, each group is homogeneous. In the Meatiq complex, the Arieki late granite presents a classical high-*K* calc-alkaline granite REE pattern (Fig. 4A), and the Abu Ziran granodiorite pattern shows the presence of cumulative feldspar (Fig. 4B). The Um Baanib orthogneiss and enclaves (Fig. 4C), respectively, show patterns similar to the Arieki granite and the Abu Ziran granodiorite, suggesting that the calc-alkaline and alkaline groups defined above share some common characteristics. The Meatiq paragneiss samples (Fig. 4D) are enriched in REE, especially HREE. The Hafafit late granite and the migmatite (Fig. 4E) share a common pattern, in agreement with the observation that this migmatite is younger than development of gneissic foliation and lineation. Both are characterized by low HREE concentrations suggesting a garnet-rich source. The amphibolites (Fig. 4F) shows REE patterns that are typical of cumulates variably enriched by trapped melt. The Siqat foliated granite (Fig. 4G) displays a similar REE

Table 2

Sr- and Nd-isotope analyses were carried out in the isotopic geology laboratory of the Royal Museum for Central Africa in Tervuren, Belgium. A detailed description of procedures and measurements is given in Liégeois et al. (2003). The NBS987 standard gave $^{87}Sr/^{86}Sr = 0.710252 \pm 0.000010$ (2σ on the mean of 12 standards, normalised to $^{86}Sr/^{88}Sr = 0.1194$) and the Merck Nd standard gave $^{143}Nd/^{144}Nd = 0.511738 \pm 0.000008$ (2σ on the mean of 12 standards, normalised to $^{146}Nd/^{144}Nd = 0.7219$) during the course of this study. All measured ratios have been normalised to the recommended values of 0.710250 for NBS987 and 0.511735 for Nd Merck standard (corresponding to a La Jolla value of 0.511858) based on the 4 standards measured on each turret together with 16 samples. Decay constant for ^{87}Rb (1.42×10^{-11} a^{-1}) was taken from Steiger and Jäger (1977) and for ^{147}Sm (6.54×10^{-12} a^{-1}) from Lugmair and Marti (1978). The references for the zircon ages are: (1) Andresen et al. (2009); (2) Loizenbauer et al.(2001); and (3) Kröner et al. (1994). A number within bracket means "by extrapolation from" (see text). ε_{Nd}(Zr-age) means that the ε_{Nd} has been calculated at the zircon age given in the first column of the table. I_{DM} ages calculated following Nelson and Depaolo (1985).

Zircon age	Ref	Sample	Rb	Sr	$^{87}Rb/^{86}Sr$	$^{87}Sr/^{86}Sr$	2σ	Sri_{600Ma}	Sm	Nd	$^{147}Sm/^{144}Nd$	$^{143}Nd/^{144}Nd$	2σ	$\varepsilon_{Nd(0Ma)}$	$\varepsilon_{Nd(Zr-age)}$	T_{DM}
590 ± 3	1	EB16	157.4	86.6	5.27	0.730011	0.000010	0.68490	6.28	29.5	0.1287	0.512625	0.000013	−0.25	4.88	762
590 ± 3	1	EB17	139.3	116	3.50	0.745506	0.000009	0.71556	7.24	36.8	0.1190	0.512610	0.000015	−0.55	5.32	710
606 ± 1	1	EB1	39.3	1078	0.11	0.703557	0.000008	0.70266	4.82	26.1	0.1118	0.512626	0.000013	−0.23	6.35	638
630 ± 2	1	EB3	70.4	30.1	6.80	0.757602	0.000014	0.69941	18.1	90.9	0.1205	0.512642	0.000009	0.08	6.23	670
630 ± 2	1	EB6	61.7	18.9	9.54	0.783822	0.000016	0.70217	18.9	85.5	0.1337	0.512657	0.000008	0.37	5.45	749
630 ± 2	1	EB7	140.1	6.8	62.44	1.218607	0.000024	0.68433	17.6	67.7	0.1576	0.512816	0.000006	3.47	6.63	642
630 ± 2	1	EB4	9.6	312	0.09	0.703730	0.000008	0.70296	6.04	25.3	0.1447	0.512704	0.000011	1.29	5.49	763
630 ± 2	1	EB8	10.6	458	0.07	0.703147	0.000011	0.70258	9.25	45.6	0.1228	0.512664	0.000008	0.51	6.47	651
779 ± 4	2	EB9	181.4	13.4	41.43	1.290719	0.000015	0.93626	66.6	266	0.1512	0.512715	0.000009	1.50	6.05	813
779 ± 4	2	EB10	76.5	31.8	6.99	0.763011	0.000010	0.70316	24.0	127	0.1145	0.512574	0.000013	−1.25	6.96	732
677 ± 9	3	EB18	181.7	75.4	7.01	0.762634	0.000009	0.70266	8.99	40.9	0.1330	0.512608	0.000021	−0.59	4.94	831
677 ± 9	3	EB19	164.9	75.4	6.36	0.757530	0.000010	0.70313	10.36	50.0	0.1253	0.512682	0.000010	0.86	7.05	639
677 ± 9	3	EB20	153.7	74.7	5.98	0.754156	0.000007	0.70298	9.21	42.1	0.1323	0.512655	0.000012	0.33	5.92	740
677 ± 9	3	EB22	198.2	75.4	7.65	0.769009	0.000010	0.70353	7.57	39.9	0.1147	0.512599	0.000006	−0.76	6.34	696
677 ± 9	3	EB23	212.5	76.9	8.05	0.774718	0.000018	0.70582	11.8	58.3	0.1226	0.512627	0.000012	−0.21	6.21	709
677 ± 9	3	EB24	164.2	69.5	6.87	0.760777	0.000005	0.70199	9.93	44.8	0.1341	0.512645	0.000010	0.14	5.56	774
700 ± 12	3	EB27	61.0	137	1.29	0.714370	0.000014	0.70336	3.78	21.3	0.1070	0.512549	0.000009	−1.74	6.30	717
700 ± 12	3	EB33	31.5	26.1	3.51	0.733150	0.000009	0.70313	4.50	27.5	0.0988	0.512519	0.000008	−2.32	6.45	706
700 ± 12	3	EB34	36.9	50.0	2.14	0.719509	0.000007	0.70124	4.64	31.5	0.0891	0.512472	0.000010	−3.24	6.40	709
700 ± 12	3	EB26	9.3	352	0.08	0.703321	0.000007	0.70267	1.28	4.40	0.1754	0.512939	0.000008	5.87	7.79	–
700 ± 12	3	EB35	7.6	169	0.13	0.703418	0.000009	0.70231	0.82	2.20	0.2239	0.513105	0.000012	9.11	6.69	–
700 ± 12	3	EB36	12.4	466	0.08	0.703471	0.000008	0.70281	4.84	20.1	0.1458	0.512927	0.000018	5.64	10.21	–
677 ± 9	3	EB30	37.9	31.9	3.45	0.730585	0.000009	0.70109	17.2	76.5	0.1359	0.512715	0.000016	1.50	6.41	660
677 ± 9	3	EB31	37.8	77.1	1.42	0.714398	0.000009	0.70225	24.6	134	0.1108	0.512578	0.000010	−1.17	5.76	701
601 ± 13	(1)	EB29	33.5	251	0.39	0.705615	0.000012	0.70231	4.24	27.6	0.0929	0.512588	0.000011	−0.98	7.01	588
601 ± 13	(1)	EB32	44.4	33.2	3.88	0.735897	0.000009	0.70273	26.2	144	0.1100	0.512655	0.000009	0.33	7.00	586
601 ± 13	(1)	EB37	44.2	21.2	6.06	0.753870	0.000012	0.70201	23.7	122	0.1172	0.512679	0.000010	0.80	6.92	592

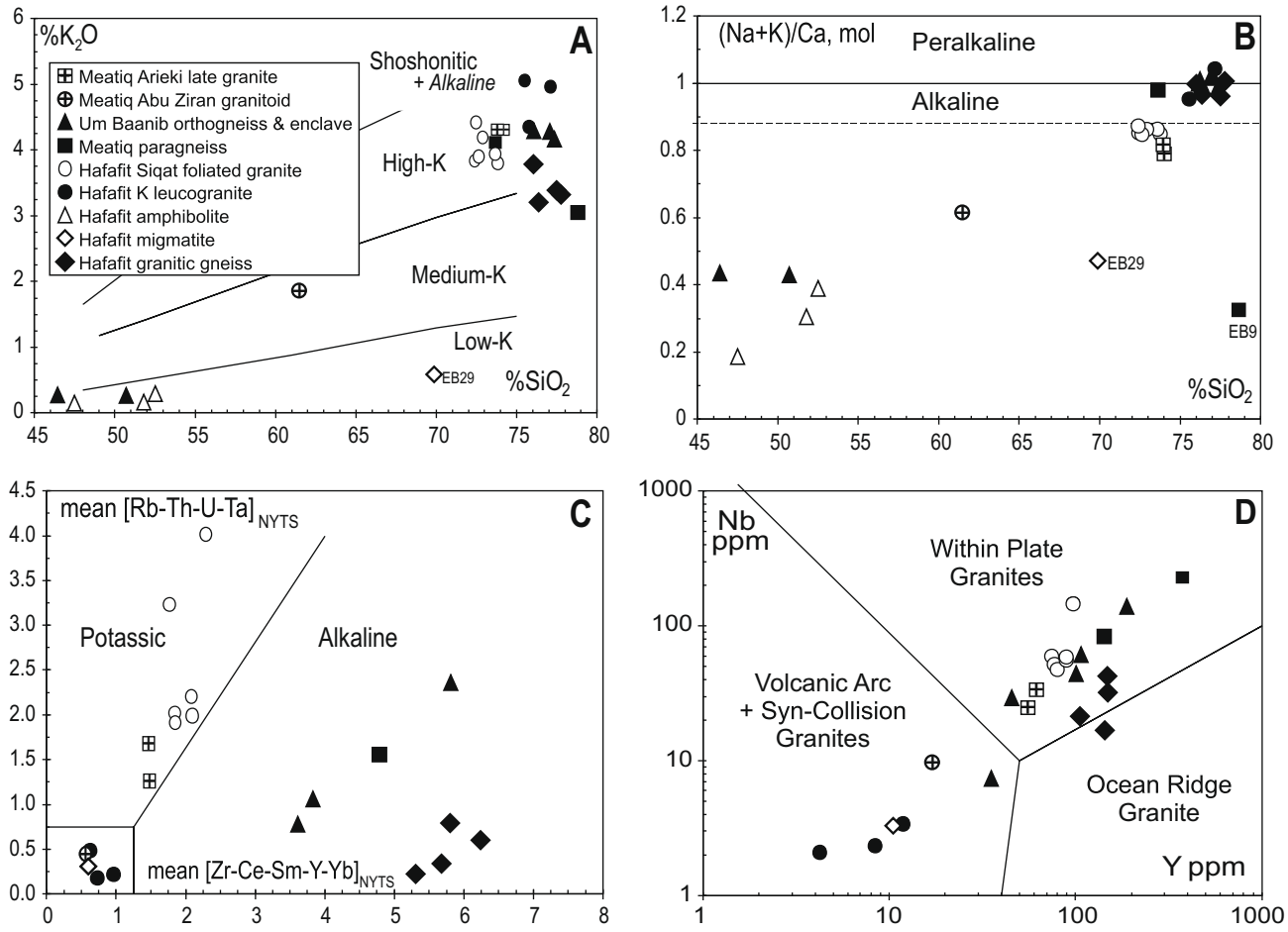

Fig. 3. Some major and trace elements of the studied rocks: (A) SiO_2 vs K_2O in weight% (boundaries from Peccerillo and Taylor (1976)); (B) SiO_2 vs (Na + K)/Ca in molar proportion (peralkaline index); peralkaline rocks have an peralkaline index >1 while other alkaline rocks are generally above 0.87 (Liégeois and Black (1987)); (C) Representation of the studied samples normalised (sliding normalization) to the Yenchichi–Telabit Series (NYTS) in a diagram differentiating the potassic and the alkaline series (Liégeois et al. (1998)); and (D) Tectonic discrimination diagram using immobile elements for granitoids (Pearce et al. (1984)).

pattern to the Arieki granite. The Hafafit granitic gneisses (Fig. 4H) are enriched in REE but do not display patterns that are very different from the Siqat granites.

4. Rb–Sr and Sm–Nd isotopic results: only Neoproterozoic protoliths

Data and analytical techniques can be found in Table 2.

4.1. Rb–Sr isochrons and Sr initial ratios

As discussed previously, the main deformation event at Meatiq is 610–605 Ma (Andresen et al., 2009). This existence of a major tectonic event at this time in Eastern Desert is confirmed by our Rb–Sr isotopic data (Fig. 5): Hafafit gneissic granitoids give a Rb–Sr isochron age of 609 ± 17 Ma (14 WR, MSWD = 3.6, initial $^{87}Sr/^{86}Sr = 0.7021 \pm 0.0009$). Adding the Um Baanib orthogneiss from the Meatiq complex does not significantly change the result: 596 ± 15 Ma (17 WR, MSWD = 3.6, initial $^{87}Sr/^{86}Sr = 0.7026 \pm 0.0011$). The five amphibolites (three from Hafafit, two from Meatiq) and the Meatiq Abu Ziran granodiorite are very close to the origin of this composite isochron. One Meatiq metasediment lies on the isochron (EB10) while the other, with very high Rb/Sr, lies above. The existence of this composite isochron suggests that the Rb–Sr geochronometer has been reset during the late Neoproterozoic c. 600 Ma Pan-African thermal event, perhaps related to Najd strike-slip deformation (Fritz et al., 1996; Kusky and Matsah, 2003). The low initial $^{87}Sr/^{86}Sr$ for all Meatiq and Hafafit samples, even those with high $^{87}Rb/^{86}Sr$, is a strong indication that this resetting occurred shortly after the intrusion of various juvenile protoliths. This renders very dangerous the calculation of selected samples as Khudeir et al. (2008) did for Sikait gneissose rocks in their Fig. 8: they arrive at an age of 677 Ma with an unrealistic initial $^{87}Sr/^{86}Sr$ (Sr_i below 0.7); we note that these authors claim an error of ±10 Ma for this age while the actual error is ±110 Ma (using the same Isoplot software as these authors).

Table 2 also reports initial $^{87}Sr/^{86}Sr$ (Sr_i) for all samples. Because the calculation of Sr_i is very sensitive to small errors in $^{87}Rb/^{86}Sr$ and age, Sr_i for samples with high $^{87}Rb/^{86}Sr$ are unreliable. Accepting Sr_i for samples with $^{87}Rb/^{86}Sr < 3$ yields 10 samples with Sr_i ranging from 0.70124 to 0.70336. A mean value of 0.70252 ± 0.00056 (one standard deviation) is obtained for these 10, which is very similar to what would be expected for magmas extracted from depleted mantle during the Neoproterozoic and much lower than what would be expected if there was even minor involvement of pre-Neoproterozoic continental crust.

4.2. Epsilon Nd and T_{dm} Nd model ages

Table 2 lists ε_{Nd} values for 27 samples (10 from Meatiq and 17 from Hafafit), each calculated using the best available crystallization age. These are all positive and range from +4.9 to +10.2, with

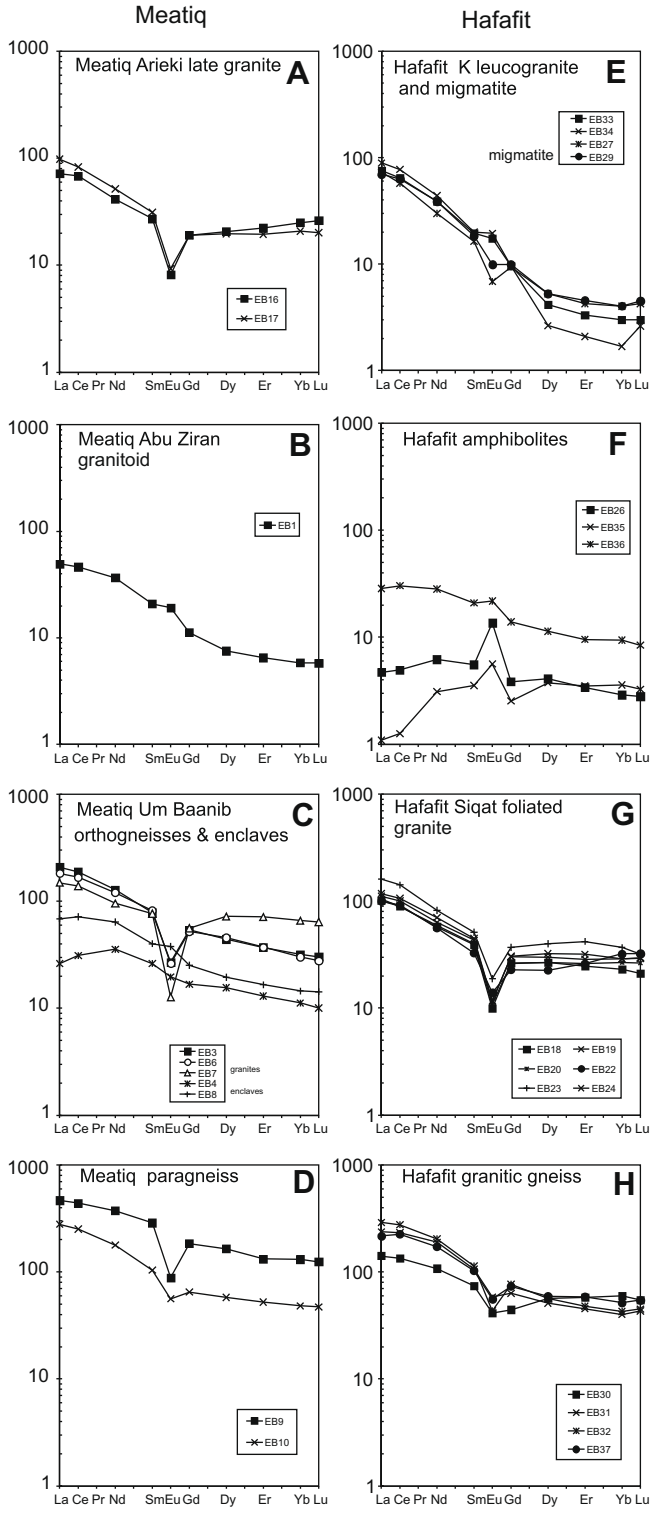

Fig. 4. REE diagrams for the studied rocks. Normalization to chondrites following Taylor and McLennan (1985).

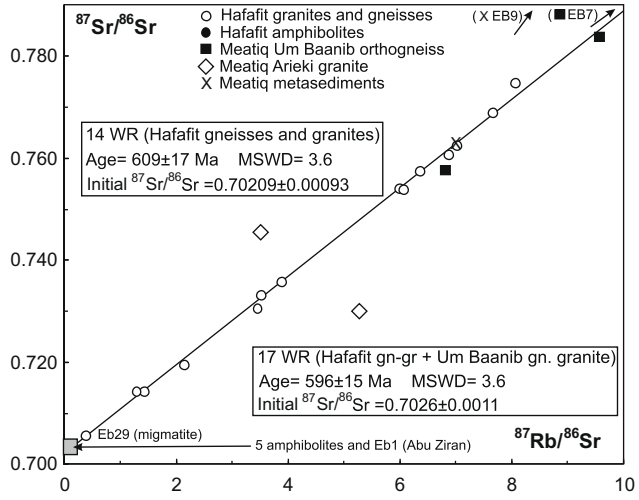

Fig. 5. Rb–Sr isochron diagram. The 14-points whole-rock (WR) isochron has been calculated on all gneissic, migmatitic and granitic lithologies, i.e., all samples except the amphibolites from the Hafafit complex; the 17 WR isochron has been calculated on the same samples with in addition the 3 Um Baanib orthogneiss from the Meatiq complex. Ages calculated with Isoplot three (Ludwig (2003)).

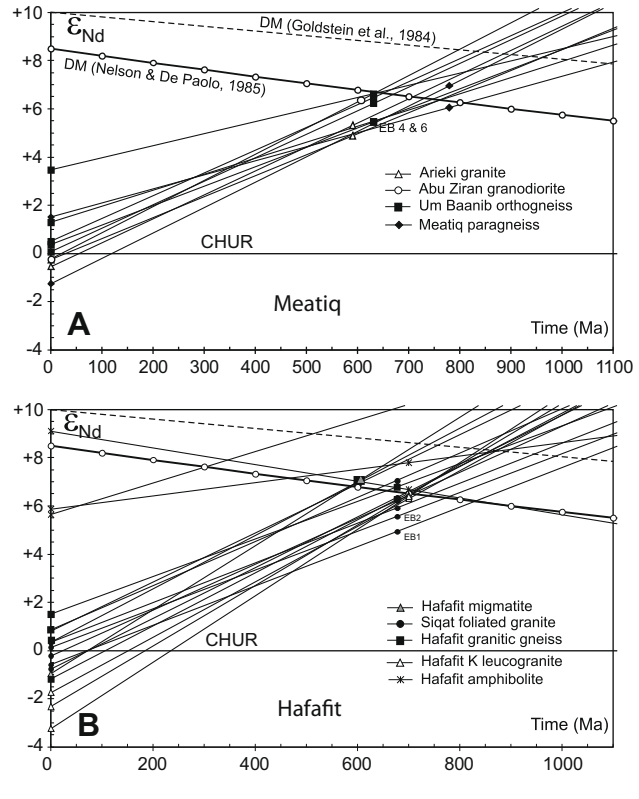

Fig. 6. Nd isotopic evolution through time for (A) the Meatiq samples (A) and (B) the Hafafit samples displaying the T_{DM} model ages (intersection with the Nelson and DePaolo (1985) evolution curve for the depleted mantle). The various symbols present on the evolution lines are placed at the zircon age inferred for the considered sample (see Table 2). CHUR = chondritic uniform reservoir; DM = depleted mantle. The Goldstein et al. (1984) depleted mantle curve is shown as a dashed line for reference.

a mean of +6.4 ± 1.0 (one standard deviation). The vast majority of these samples are between +5 and +7; all of these data indicate derivation from a source with a time-integrated depletion in Nd relative to Sm, consistent with an interpretation that, prior to the Neoproterozoic, Nd evolved in a strongly depleted, upper-mantle-like chemical reservoir. Significant involvement of pre-Neoproterozoic crust should result in a strongly negative ε_{Nd}, and this is not observed for any gneiss sample that we analyzed.

For determining the mean age of the protolith of a geological unit, either magmatic or sedimentary, Nd T_{DM} model ages are a very powerful tool (DePaolo, 1983) as these consider the whole-rocks and thus magma sources. The principle of the method is to calculate at what age the sample had the $^{143}Nd/^{144}Nd$ of the

depleted mantle, thus approximating the extraction of the melt (and fractionation of Sm/Nd) from its source. This requires a realistic model for the depleted mantle. There are two models for the depleted mantle that are widely used, those of DePaolo (1981, 1983) and Goldstein et al. (1984). The DePaolo and Goldstein models differ in that the latter is linear between ε_{Nd} = +10 today ε_{Nd} = 0 at 4.6 Ga, whereas the former model is a quadratic expression that uses ε_{Nd} = +8.5 for modern juvenile crust. Using these different algorithms yields different model ages, with Goldstein model ages being 100–200 million years older than DePaolo model ages for Neoproterozoic rocks.

We prefer the evolution curve based on oceanic island arcs proposed by DePaolo (1981, 1983); (Nelson and DePaolo, 1985), for reasons discussed by Stern (2002). Nd T_{DM} model age calculations also assume that the $^{147}Sm/^{144}Nd$ of the rock remained constant since its generation (REE are difficult to mobilize except in melts) and that it was derived from a depleted mantle that is isotopically approximated by the model. Complications occur if enriched lithospheric mantle was the magma source, or if the igneous rocks were generated from partial melting of much older crust. In such cases a two-stage calculation can be performed, but this is not needed here, nor would such a calculation lead to significantly different Nd model ages for Meatiq–Hafafit samples. It is also important to calculate Nd model ages for samples with low $^{147}Sm/^{144}Nd$ (LREE-enriched) so that the corrected sample trajectory intersects the mantle evolution curve at a high angle; Stern (2002) used a filter of $^{147}Sm/^{144}Nd < 0.165$; we exclude two Hafafit amphibolite samples (EB-26 and EB-35) for T_{DM} calculation on this basis as well as EB36 with a rather high $^{147}Sm/^{144}Nd$ (0.146) and an obviously too young T_{DM} (304 Ma) but show these samples on Fig. 6. In Fig. 6, the evolution through time of the sample $^{143}Nd/^{144}Nd$ (expressed as ε_{Nd},$(^{143}Nd/^{144}Nd)_{sample,t}/(^{143}Nd/^{144}Nd)_{CHUR,t} - 1$; t = considered age and CHUR = chondritic uniform reservoir, equivalent to the Bulk Earth) is shown with the depleted mantle evolution curve and CHUR. The T_{DM} model age is given by the intersection of the sample line with the DM curve and reported for each sample in Table 2.

Fig. 7 compares the new Nd model ages for Meatiq and Hafafit with existing ages for the Eastern Desert (Stern, 2002). A mean T_{DM} of 0.70 Ga with a remarkably small standard deviation of 0.07 Ga is obtained for the 23 model ages listed in Table 2. Means for nine Meatiq samples (0.71 ± 0.06) and 14 Hafafit samples (0.69 ± 0.07) are statistically indistinguishable. This is very close to the mean T_{DM} of 0.74 ± 0.17 Ga reported for 56 Eastern Desert samples by Stern (2002), who concluded (p. 112): "The juvenile nature of the crust is confirmed by the Nd model ages from this region, which shows a tight clustering of crust formation ages very close to the crystallization ages of the same rocks". Data for Egypt and Sudan cluster tightly about model ages of ~750 million years, and convincingly demonstrate that these crusts are dominated by juvenile additions from the mantle during Neoproterozoic time. The same conclusion applies to the results reported here. There may be a minor contribution of much older crust and/or sediments that cannot be identified isotopically, but significant contributions of older materials should result in a larger spread of Nd model ages reflecting a mixture between juvenile crustal additions and older crust. A similar variability and shift towards more radiogenic values should also be observed for initial $^{87}Sr/^{86}Sr$ values, which instead also cluster tightly around values expected for Neoproterozoic asthenospheric mantle.

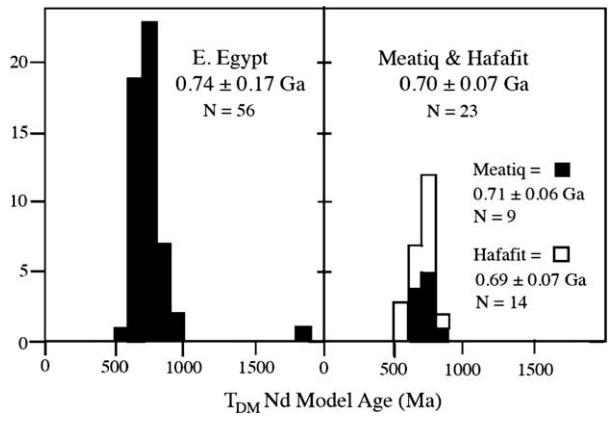

Fig. 7. Histograms of Nd model ages for (a) Egypt east of the Nile, excluding Sinai (from Stern (2002)). (b) Meatiq and Hafafit gneisses, reported here. Bold numbers are means for the population ±1 standard deviation. Note that Nd model ages for Eastern Desert samples approximate crystallization ages, as expected for juvenile crust. Meatiq and Hafafit gneisses cannot be distinguished from most other rocks from the Eastern Desert, including demonstrably primitive ophiolites and mafic arc volcanics.

Because none of the expected isotopic indicators of pre-Neoproterozoic crustal involvement are seen for any of the Meatiq and Hafafit samples, we conclude that statements such as that of Khudeir et al. (2008, p. 104): "The positive ε_{Nd} values estimated for all (Meatiq and Hafafit) gneissic granites are best explained as resulting from interaction of mantle-derived melts with crustal components of the pre-Neoproterozoic continent" must be rejected as completely unsupported. These authors suggest that percolation of Nd through nearby juvenile ANS rocks somehow overprinted the old Nd isotopic signature of a pre-Neoproterozoic crust to form the epsilon Nd values of the Meatiq and Hafafit gneisses. Such a process has not been described anywhere and is not expected from theoretical considerations. REE are mobilized by melting and can be mobilized during metamorphism under certain conditions, as occurred in the 2 Ga basement of the northern boundary of the West African craton during the late Neoproterozoic (Ennih and Liégeois, 2008). However, in that case, all REE were affected, which is not the case here (Fig. 4) and the radiogenic ^{143}Nd accumulated since the crystallization of the 2 Ga rocks is still present. Moreover, reasonable Nd T_{DM} model ages are found if two-stage calculations are used. Radiogenic ^{143}Nd cannot be selectively removed as can radiogenic Pb be removed from zircon because the crystallographic site of ^{147}Sm is also appropriate for radiogenic ^{143}Nd, which is much less the case of radiogenic Pb present in the crystallographic site of U.

The Nd isotope results presented here are very coherent and indicate unambiguously that the protolith of the Meatiq and Hafafit gneissic complexes are juvenile late Neoproterozoic rocks.

5. The problem of pre-Neoproterozoic inherited zircons

The Nd and Sr isotopic data indicate that Meatiq and Hafafit gneisses are juvenile crust, a conclusion that is supported by geochronological studies discussed earlier. There is evidence, also discussed previously, that pre-Neoproterozoic zircons occur especially in Eastern Desert mafic metavolcanic rocks (Ali et al., 2009b), and these two conflicting observations present an important paradox. Inherited zircons dated by TIMS, SHRIMP or laser ICP-MS provide robust ages but these relate to the age of the mineral, not the rock; combining both U–Pb zircon and Sm–Nd whole-rock methods is obviously the best way to assess whether or not the crust is juvenile and the extent to which it has interacted with ancient crust or sediments (e.g., Küster et al. (2008) for central Sudan). In Eastern Desert, the existence of pre-Neoproterozoic inherited zircons apparently contradicts the Sr and Nd isotope evidence for juvenile crust. This paradox clearly exists for the Arabian–Nubian Shield and may be present for other tracts of Neoproterozoic

juvenile crust, such as the Central Asian Orogenic Belt (Kröner et al., 2007). This apparent contradiction can be solved by closely examining the nature of the information. The Sr and Nd isotopic compositions relate to the considered magma and its source. If enough lithologies of an area are analyzed for Sr and Nd isotopic compositions, the latter can be considered as representative of the studied crust. This is not the case for inherited zircons: zircon is a very resilient mineral, difficult to dissolve or to destroy and, except in alkaline-peralkaline environment, it keeps the memory of the different stages of crystallization that it experienced (e.g., Bendaoud et al., 2008). Zircon can survive in the mantle up to 1500 °C and 20 GPa, equivalent to 600 km deep in the Earth (Tange and Takahashi, 2004). Some detrital zircons carried by deep subduction into the diamond zone survive (Claoué-Long et al., 1991; Hermann et al., 2001), as well as zircons that formed in the oceanic crust itself (Usui et al., 2003). Zircons formed in the crust may also be carried into the mantle by delamination of dense lower crust (Kay and Kay, 1993). Regardless of how zircons formed in the crust are introduced into the mantle, they are resilient enough to even survive extensive melting and be carried back to the surface in magmas. This is the simplest explanation for the presence of inherited ancient zircons documented for mid-Atlantic ridge MORB-type gabbros (Pilot et al., 1998; Belyatsky et al., 2008). This is probably the origin of inherited zircons found in some ophiolites (e.g., Whattam et al., 2006), including the Neoproterozoic Thurwah ophiolite of Saudi Arabia (Pallister et al., 1988; Hargrove et al., 2006a). Old zircons can also be incorporated in magmas when these incorporate clastic sediments (e.g., Ali et al., 2009b; Hargrove et al., 2006a). Regardless of the precise way in which old zircons become xenocrysts in younger igneous rocks, it is clear that this can occur in mantle-derived melts and thus be incorporated in juvenile crust, without the need that significant tracts of ancient crust existed at the site of juvenile crust formation. This demonstrates that combining U–Pb zircon ages and Nd T_{DM} model ages is highly powerful (e.g., Zhang et al., 2005; Küster et al., 2008).

6. Conclusions

These results show without ambiguity that the story of the Meatiq and Hafafit complexes concerns the building of a mostly 750–600 Ma old tract of juvenile crust, perhaps the crust of an oceanic island arc, which was largely remobilized during the ~600 Ma collision and related strike-slip shearing leading to Greater Gondwana supercontinent formation (Stern, 2008). There was no discernible participation of pre-Neoproterozoic crust. The remelting of a slightly older juvenile crust can explain the felsic nature and chemical variability (from potassic to alkaline) of the studied rocks (Fig. 3), which could result from different degrees of partial melting. Geochemistry gives indications about the nature of the magma source but geotectonic inferences are partly model-dependant (Liégeois et al., 1998). The late Neoproterozoic T_{DM} model ages of late granites such as Abu Ziran (606 Ma) and Arieki (590 Ma) are most consistent with the inference that no pre-Neoproterozoic crust exists below the Eastern Desert of Egypt, coherent with the U–Pb zircon and Sm–Nd isotopic results for similar granites by Moussa et al. (2008). The existence of some pre-Neoproterozoic inherited zircons does not contradict that conclusion: old zircons can be introduced in juvenile magmas through several ways without requiring the participation of ancient crust itself. We see no support for the hypothesis that ancient crust lies beneath the Eastern Desert. The eastern boundary of the Saharan metacraton must lie further west.

The Sr- and Nd-isotopic dataset for Meatiq and Hafafit gneisses indicates clearly that these gneisses are juvenile Neoproterozoic crustal additions and that the important metamorphic event recorded in the Eastern Desert gneissic domes is related to the main Neoproterozoic Pan-African orogeny at c. 600 Ma corresponding to the formation of Greater Gondwana.

Acknowledgements

We thank A.A. Khudeir and M.A. Abu El Rus from the Assiut University for showing one of us (JPL) these gneissic complexes in 1993. Interesting remarks by Bernard Bonin contributed to strengthening this work. Finally, we warmly thank Richard Hanson for his detailed review that allowed us to further improve this paper and the second reviewer for his positive advice.

References

Abdel-Monem, A.A., Hurley, P.M. 1979. U–Pb Dating of Zircons from Psammitic Gneisses, Wadi Abu Rosheid-Wadi Sikait area, Egypt. Institute of Applied Geology, King Abdulaziz University Jeddah, Bulletin, vol. 3, pp. 165–70.

Abd El-Naby, H., Frisch, W., 2006. Geochemical constraints from the Hafafit metamorphic complex (HMC): evidence of neoproterozoic back-arc basin development in the central eastern desert of Egypt. Journal of African Earth Sciences 45, 173–186.

Abdelsalam, M.G., Stern, R.J., 1996. Sutures and shear zones in the Arabian–Nubian shield. Journal of African Earth Sciences 23, 289–310.

Abdelsalam, M.G., Liégeois, J.P., Stern, R.J., 2002. The Saharan metacraton. Journal of African Earth Sciences 34, 109–117.

Ali, K.A., Stern, R.J., Manton, W.I., Johnson, P.R., Mukherjee, S.K., 2009a. Neoproterozoic diamictite in the Eastern Desert of Egypt and Northern Saudi Arabia: evidence of ~750 Ma glaciation in the Arabian–Nubian shield. International Journal of Earth Sciences. doi:10.1007/s00531-009-0427-3.

Ali, K.A., Stern, R.J., Manton, W.I., Kimura, J.I., Khamees, H.A., 2009b. Geochemistry, Nd isotopes and U–Pb SHRIMP zircon dating of Neoproterozoic volcanic rocks from the Central Eastern Desert of Egypt: new insights into the ~750 Ma crust-forming event. Precambrian Research 171, 1–22.

Andresen, A., El-Rus, M.M.A., Myhre, P.I., Boghdady, G.Y., Corfu, F., 2009. U–Pb TIMS age constraints on the evolution of the Neoproterozoic Meatiq Gneiss Dome, Eastern Desert, Egypt. International Journal Earth Sciences 98, 481–497.

Belyatsky, B., Lepekhina, E., Antonov, A., Shuliatin, O., Sergeev, S. 2008. Age and Genesis of Accessory Zircon from MAR Gabbroids. Geophysical Research Abstracts 10, EGU2008-A-01314 (abstract).

Bendaoud, A., Ouzegane, K., Godard, G., Liégeois, J.P., Kienast, J.R., Bruguier, O., Drareni, A., 2008. Geochronology and metamorphic P–T–X evolution of the Eburnean granulite-facies metapelites of Tidjenouine (Central Hoggar, Algeria): witness of the LATEA metacratonic evolution. In: Ennih, N., Liégeois, J.-P. (Eds.), The Boundaries of the West African Craton, vol. 297. Special Publications, Geological Society, London, pp. 111–146.

Bregar, M., Bauernhofer, A., Pelz, K., Kloetzli, U., Fritz, H., Neumayr, P., 2002. A late Neoproterozoic magmatic core complex in the Eastern Desert of Egypt: emplacement of granitoids in a wrench-tectonic setting. Precambrian Research 118, 59–82.

Claoué-Long, J.C., Sobolev, N.V., Shatsky, V.S., Sobolev, A.V., 1991. Zircon response to diamond-pressure metamorphism in the Kokchetav massif, USSR. Geology 19, 710–713.

DePaolo, D.J., 1981. Neodymium isotopes in the Colorado Front Range and crust-mantle evolution in the Proterozoic. Nature 291, 193–196.

DePaolo, D.J., 1983. The mean life of continents: estimates of continent recycling rates from Nd and Hf isotopic data and implications for mantle structure. Geophysical Research Letters 10, 705–708.

El-Gaby, S., El-Nady, O.M., Khudeir, A.A., 1984. Tectonic evolution of the basement complex in the CED of Egypt. Geologishe Rundschau 73, 1019–1036.

Ennih, N., Liégeois, J.P., 2008. The boundaries of the West African craton, with a special reference to the basement of the Moroccan metacratonic Anti-Atlas belt. In: Ennih, N., Liégeois, J.-P. (Eds.), The Boundaries of the West African Craton, vol. 297. Special Publications, Geological Society, London, pp. 1–17.

Fowler, A.-R., El Kalioubi, B., 2002. The Migif–Hafafit gneissic complex of the Egyptian Eastern Desert: fold interference patterns involving multiply deformed sheath folds. Tectonophysics 346, 247–275.

Fowler, A.R., Khamees, H., Dowidar, H., 2007. El Sibai gneissic complex, Central Eastern Desert, Egypt: folded nappes and syn-kinematic gneissic granitoid sheets – not a core complex. Journal of African Earth Sciences 49, 119–135.

Fritz, H., Wallbrecher, E., Khudeir, A.A., Abu El Ela, F., Dallmeyer, D.R., 1996. Formation of Neoproterozoic metamorphic core complexes during oblique convergence (Eastern Desert, Egypt). Journal of African Earth Sciences 23, 311–329.

Fritz, H., Dallmeyer, D.R., Wallbrecherr, E., Loizenbauer, J., Hoinkes, G., Neumayr, P., Khudeir, A.A., 2002. Neoproterozoic tectonothermal evolution of the Central Eastern Desert, Egypt: a slow velocity tectonic process of core complex exhumation. Journal of African Earth Sciences 34, 137–155.

Goldstein, S.L., O'Nions, R.K., Keith, R., Hamilton, P.J., 1984. A Sm–Nd isotopic study of atmospheric dusts and particulates from major river systems. Earth Planetary Science Letters 70, 221–236.

Hadj Kaddour, Z., Liégeois, J.P., Demaiffe, D., Caby, R., 1998. The alkaline-peralkaline granitic post-collisional Tin Zebane dyke swarm (Pan-African Tuareg shield, Algeria): prevalent mantle signature and late agpaitic differentiation. Lithos 45, 223–243.

Hargrove, U.S., Stern, R.J., Griffin, W.R., Johnson, P.R., Abdelsalam, M.G., 2006a. From Island Arc to Craton: Timescales of Crustal Formation along the Neoproterozoic Bi'r Umq Suture Zone, Saudi Geological Survey, Kingdom of Saudi Arabia, p. 69.

Hargrove, U.S., Stern, R.J., Kimura, J.-I., Manton, W.I., Johnson, P.R., 2006b. How juvenile is the Arabian–Nubian shield? Evidence from Nd isotopes and pre-Neoproterozoic inherited zircon in the Bi'r Umq suture zone, Saudi Arabia. Earth and Planetary Science Letters 252, 308–326.

Harris, N.B.W., Hawkesworth, C.J., Ries, A.C., 1984. Crustal evolution in north-east and East Africa from model Nd ages. Nature 309, 773–776.

Hermann, J., Rubatto, D., Korsakov, A., Shatsky, V., 2001. Multiple zircon growth during fast exhumation of diamondiferous, deeply subducted continental crust (Kokchetav Massif, Kazakhstan). Contributions Mineralogy Petrology 141, 66–82.

Hume, W. 1934. Geology of Egypt, the Fundamental Pre-Cambrian Rocks of Egypt and the Sudan, their Distribution, Age, and Character. Part 1. The Metamorphic Rocks, vol. 1. Egyptian Government Printing Office.

Johnson, P.R., Woldehaimanot, B., 2003. The Arabian–Nubian shield in a Gondwana context: a review of accretion and deformation in the northern East African Orogen. In: Yoshida, M. et al. (Eds.), Proterozoic East Gondwana: Supercontinent Assembly and Breakup, vol. 206. Special Publication, Geological Society, London, pp. 289–325.

Kay, R.W., Kay, S.M., 1993. Delamination and delamination magmatism. Tectonophysics 219, 177–189.

Kennedy, A., Johnson, P.R., Kattan, F. H., 2004. SHRIMP Geochronology in the Northern Arabian Shield. Part I: Data Acquisition: Saudi Geological Survey Open File Report, v. SGS-OF-2004-11.

Kennedy, A., Johnson, P.R., Kattan, F.H., 2005, SHRIMP Geochronology in the Northern Arabian Shield. Part II: Data Acquisition 2004: Saudi Geological Survey Open File Report, v. SGS-OF-2005-10.

Kennedy, A., Johnson, P.R., Kattan, F.H., 2007. SHRIMP Geochronology in the Northern Arabian Shield: Part III Data Acquisition, 2006, Jeddah, Saudi Geological Survey.

Khudeir, A.A., Abu El-Rus, M.A., El-Gaby, S., El-Nady, O., Bishara, W.W., 2008. Sr–Nd isotopes and geochemistry of the infrastructural rocks in the Meatiq and Hafafit core complexes, Eastern Desert, Egypt: evidence for involvement of pre-Neoproterozoic crust in the growth of Arabian–Nubian shield. Island Arc 17, 90–108.

Kröner, A., Krüger, J., Rashwan, A.A.A., 1994. Age and tectonic setting of granitoid gneisses in the Eastern Desert of Egypt and south-west Sinai. Geologische Rundschau 83, 502–513.

Kröner, A., Windley, B.F., Badarach, G., Tomurtogoo, O., Hegner, E., Jahn, B.M., Gruschka, S., Khain, E.V., Demoux, A., Wingate, M.T.D., 2007. Accretionary growth and crust formation in the Central Asian Orogenic Belt and comparison with the Arabian–Nubian Shield. In: Hatcher, Jr., R.D., Carlson, M.P., McBride, J.H., Martínez Catalán, J.R., (Eds.), 4-D Framework of Continental Crust: Geological Society of America Memoir 200, GSA Memoir 200, pp. 181–209.

Kusky, T.M., Matsah, M.I., 2003. Neoproterozoic Dextral Faulting on the Najd Fault System, Saudi Arabia, Preceeded Sinistral Faulting and Escape Tectonics Related to the Closure of the Mozambique Ocean, vol. 206. Geological Society, Special Publications, London, pp. 327–361.

Küster, D., Liégeois, J.-P., 2001. Sr, Nd isotopes and geochemistry of the Bayuda Desert high-grade metamorphic basement (Sudan): an early Pan-African oceanic convergent margin, not the edge of East Saharan ghost craton? Precambrian Research 109, 1–23.

Küster, D., Liégeois, J.P., Matukov, D., Sergeev, S., Lucassen, F., 2008. Zircon geochronology and Sr, Nd, Pb isotope geochemistry of granitoids from Bayuda Desert and Sabaloka (Sudan): evidence for a Bayudian event (920–900 Ma) preceding the Pan-African orogenic cycle (860–590 Ma) at the eastern boundary of the Saharan Metacraton. Precambrian Research 164, 16–39.

Liégeois, J.-P., Black, R., 1987. Alkaline magmatism subsequent to collision in the Pan-African belt of the Adrar des Iforas. In: Fitton, J.G., Upton, B.G.J. (Eds.), Alkaline Igneous Rocks, vol. 30. Blackwell Scientific Publications, The Geological Society, pp. 381–401.

Liégeois, J.P., Navez, J., Hertogen, J., Black, R., 1998. Contrasting origin of post-collisional high-*K* calc-alkaline and shoshonitic versus alkaline and peralkaline granitoids. Lithos 45, 1–28.

Liégeois, J.P., Latouche, L., Boughrara, M., Navez, J., Guiraud, M., 2003. The LATEA metacraton (Central Hoggar, Tuareg shield, Algeria): behaviour of an old passive margin during the Pan-African orogeny. Journal of African Earth Sciences 37, 161–190.

Loizenbauer, J., Wallbrecher, E., Fritz, H., Neumayr, P., Khudeir, A.A., Kloetzli, U., 2001. Structural geology, single zircon ages and fluid inclusion studies of the Meatiq metamorphic core complex: implications for Neoproterozoic tectonics in the Eastern Desert of Egypt. Precambrian Research 110, 357–383.

Ludwig, K.R., 2003. User's Manual for Isoplot/3, a Geochronological Toolkit for Microsoft Excel, vol. 14. Special Publication, Berkeley Geochronology Center. p. 71.

Lugmair, G.W., Marti, K., 1978. Lunar initial 143Nd/144Nd: differential evolution of the lunar crust and mantle. Earth and Planetary Science Letters 39, 349–357.

Moussa, E.M.M., Stern, R.J., Manton, W.I., Ali, K.A., 2008. SHRIMP zircon dating and Sm/Nd isotopic investigations of Neoproterozoic granitoids, Eastern Desert, Egypt. Precambrian Research 160, 341–356.

Nelson, B.K., Depaolo, D.J., 1985. Rapid production of continental crust 1.7 to 1.9 by ago: Nd isotopic evidence from the basement of the North American midcontinent. Geological Society of America Bulletin 96, 746–754.

Neumayer, P., Hoinkes, G., Puhl, J., Mogessie, A., Khudeir, A.A., 2004. The Meatiq dome (Eastern Desert, Egypt) a Precambrian metamorphic core complex: petrological and geological evidence. Journal Metamorphic Geology 16, 259–279.

Pallister, J.S., Stacey, J.S., Fischer, L.B., Premo, W.R., 1988. Precambrian ophiolites of Arabia: geologic settings, U–Pb geochronology, Pb-isotope characteristics, and implications for continental accretion. Precambrian Research, 38, 1–54.

Pearce, J., Harris, N.B.W., Tindle, A.G., 1984. Trace element discrimination diagrams for the tectonic interpretation of granitic rocks. Journal Petrology 25, 956–983.

Peccerillo, R., Taylor, S.R., 1976. Geochemistry of Eocene calc-alkaline volcanic rocks from the Kastamonu area, northern Turkey. Contributions to Mineralogy and Petrology 58, 63–81.

Pilot, J., Werner, C.D., Haubrich, F., Baumann, N., 1998. Palaeozoic and proterozoic zircons from the Mid-Atlantic ridge. Nature 393, 676–679.

Steiger, R.H., Jäger, E., 1977. Subcommission on geochronology: convention on the use of decay constants in geo- and cosmochronology. Earth and Planetary Sciences Letters 36, 359–362.

Stern, R.J., 2002. Crustal evolution in the East African Orogen: a neodymium isotopic perspective. Journal of African Earth Sciences 34, 109–117.

Stern, R.J., 2008. Neoproterozoic crustal growth: the solid earth system during a critical episode of earth history. Gondwana Research 14, 33–50.

Stern, R.J., Hedge, C.E., 1985. Geochronologic constraints on late Precambrian crustal evolution in the Eastern Desert of Egypt. American Journal of Science 285, 97–127.

Stern, R.J., Kröner, A., Bender, R., Reischmann, T., Dawoud, A.S., 1994. Precambrian basement around Wadi Halfa, Sudan: a new perspective on the evolution of the East Saharan Craton. Geologische Rundshau 83, 564–577.

Sturchio, N.C., Sultan, M., Batiza, R., 1983. Geology and origin of Meatiq Dome, Egypt; a Precambrian metamorphic core complex? Geology 11, 72–76.

Sturchio, N.C., Sultan, M., Sylvester, P. Batiza, R., Hedge, C., El-Shazly, E.M., Abdel-Meguid, A., 1984. Geology, age, and origin of Meatiq Dome: implications for the Precambrian stratigraphy and tectonic evolution of the Eastern Desert of Egypt. In: Al-Shanti, A.M., (Ed.), King Abdulaziz University Faculty of Earth Sciences Bull, vol. 6, pp. 127–143.

Sultan, M., Arvidson, R.E., Sturchio, N.C., Guinness, E.A., 1987. Lithologic mapping in arid regions with landsat thematic mapper data; Meatiq Dome, Egypt. GSA Bulletin 99, 748–762.

Sultan, M., Tucker, R.D., El Alfy, Z., Attia, R., Ragab, A.G., 1994. U–Pb (zircon) ages for the gneissic terrane west of the Nile, southern Egypt. Geologische Rundschau 83, 514–522.

Tange, Y., Takahashi, E., 2004. Stability of the high-pressure polymorph of zircon ($ZrSiO_4$) in the deep mantle. Physics of the Earth and Planetary Interiors 143, 223–229.

Taylor, S.R., McLennan, S.M., 1985. The composition and evolution of the continental crust: rare earth element. Evidence from sedimentary rocks. Philosophical Transfer Royal Society of London 301, 381–389.

Usui, T., Nakamaura, E., Kobayashi, K., Maruyama, S., Helmstaedt, H., 2003. Fate of the subducted Farallon plate inferred from eclogite xenoliths in the Colorado Plateau. Geology 31, 589–592.

Whattam, S.A., Malpas, J., Smith, I.E.M., Ali, J.R., 2006. Link between SSZ ophiolite formation, emplacement and arc inception, Northland, New Zealand: U–Pb SHRIMP constraints. Earth and Planetary Science Letters 250, 606–632.

Whitehouse, M.J., Stoeser, D.B., Stacey, J.S., 2001a. The Khida Terrane – geochronological and isotopic evidence for Paleoproterozoic and Archean rust in the Eastern Arabian shield. Gondwana Research 4, 200–202.

Whitehouse, M.J., Windley, B.F., Stoeser, D.B., Al-Khirbash, S., Ba-Bttat, M.A.O., Haider, A., 2001b. Precambrian basement character of Yemen and correlations with Saudi Arabia and Somalia. Precambrian Research 105, 357–369.

Zhang, R.Y., Yang, J.S., Wooden, J.L., Liou, J.G., Li, T.F., 2005. U–Pb SHRIMP geochronology of zircon in garnet peridotite from the Sulu UHP terrane, China: implications for mantle. Earth and Planetary Science Letters 237, 729–743.